Remote Sensing of Environment 231 (2019) 111264

Contents lists available at ScienceDirect

Remote Sensing of Environment

journal homepage: www.elsevier.com/locate/rse

The potential of dual-wavelength terrestrial lidar in early detection of *Ips typographus* (L.) infestation – Leaf water content as a proxy

S. Junttila[a,b,*], M. Holopainen[a,b], M. Vastaranta[b,c], P. Lyytikäinen-Saarenmaa[a], H. Kaartinen[d,e], J. Hyyppä[b,d], H. Hyyppä[b,f]

[a] Department of Forest Sciences, University of Helsinki, Latokartanonkaari 7, 00014 Helsinki, Finland
[b] Centre of Excellence in Laser Scanning Research, Finnish Geospatial Research Institute (FGI), Geodeetinrinne 2, 02430 Kirkkonummi, Finland
[c] School of Forest Sciences, University of Eastern Finland, Yliopistokatu 7, 80101 Joensuu, Finland
[d] Department of Remote Sensing and Photogrammetry, Finnish Geospatial Research Institute (FGI), Geodeetinrinne 2, 02430 Kirkkonummi, Finland
[e] Department of Geography and Geology, University of Turku, Akatemiankatu 1, 20500 Turku, Finland
[f] Department of Built Environment, Aalto University, Otakaari 4, 02150 Espoo, Finland

ARTICLE INFO

Edited by Emilio Chuvieco

Keywords:
Tree health
Dual-wavelength lidar
Terrestrial laser scanning
Leaf water content
Bark beetle infestation
Ips typographus
Multispectral lidar

ABSTRACT

Climate change is causing novel forest stress around the world due to changes in environmental conditions. Forest pest insects, such as *Ips typographus* (L.), are spreading toward the northern latitudes and are now able to produce more generations in their current range; this has increased forest disturbances. Timely information on tree decline is critical in allowing forest managers to plan effective countermeasures and to forecast potential infestation areas. Field-based infestation surveys of bark beetles have traditionally involved visual estimates of entrance holes, resin flow, and maternal-gallery densities; such estimates are prone to error and bias. Thus, objective and automated methods for estimating tree infestation status are required.

In this study, we investigated the feasibility of dual-wavelength terrestrial lidar in the estimation and detection of *I. typographus* infestation symptoms. In addition, we examined the relationship between leaf water content (measured as gravimetric water content and equivalent water thickness) and infestation severity. Using two terrestrial lidar systems (operating at 905 nm and 1550 nm), we measured 29 mature Norway spruce (*Picea abies* [L.] Karst.) trees that exhibited low or moderate infestation symptoms. We calculated single and dual-wavelength lidar intensity metrics from stem and crown points to test these metrics' ability to discriminate *I. typographus* infestation levels using regressions and linear discriminant analyses.

Across the various *I. typographus* infestation levels, we found significant differences ($p < 0.05$) in gravimetric water content, but not in equivalent water thickness due to the latter statistic's high correlation with leaf density. The results show correlations between the lidar intensity metrics and several infestation symptoms: defoliation, discoloration and resin flow. The intensity metrics explain 50% of the variation in the infestation severity (as determined in the field based on canopy and stem symptoms). The overall accuracy with three infestation classes (*no*, *low*, or *moderate*) was 66%, but the overall accuracy with two infestation classes (*not infested*, or *infested*) was 90%. The classifiers combine lidar intensity metrics from the stem and the canopy to allow for the detection of bark-beetle infestations in the early, so called green-attack stage. The intensity metrics explain part of the variations in tree-level gravimetric water content and equivalent water thickness, with adjusted R^2 values of 0.48 and 0.68, respectively. Terrestrial dual-wavelength lidar shows potential for providing objective tree-decline measurements at tree level: this method can be further used to enhance forest inventories and automate tree-vigor data collection, which has traditionally required expert knowledge.

1. Introduction

Climate change is causing novel stress to forests and individual trees (Allen et al., 2015; Allen et al., 2010; Carnicer et al., 2011; Seidl and Rammer, 2017; Sturrock et al., 2011; Wong and Daniels, 2017). Because of the longer summers and higher summer temperatures, which lead to prolonged drought periods, pest insects such as the European spruce bark beetle (*Ips typographus* L.) have more favorable survival

* Corresponding author at: Department of Forest Sciences, University of Helsinki, Latokartanonkaari 7, 00014 Helsinki, Finland.
E-mail address: samuli.junttila@helsinki.fi (S. Junttila).

https://doi.org/10.1016/j.rse.2019.111264
Received 8 January 2019; Received in revised form 11 June 2019; Accepted 15 June 2019
Available online 28 June 2019

conditions, as well as increased voltinism; this results in exponential growth of bark beetles' population densities (Faccoli, 2009; Kärvemo et al., 2016). *I. typographus* bores through the bark of mature Norway spruce (*Picea abies* [L.] Karst.) trees to the phloem region in order to excavate nuptial chambers and maternal galleries, where they can mate and lay eggs. The larvae feed on the phloem tissue, which disrupts the translocation of photosynthates within the tree. In addition to damaging the phloem, *I. typographus* carries blue-stain fungi (e.g., *Endoconidiophora polonica*), which disrupt the flow of water in the xylem, thus causing the infested tree to die back (Linnakoski et al., 2017; Wermelinger, 2004). *E. polonica* causes a rapid decline in leaf water content (LWC) in Norway spruce seedlings (Junttila et al., 2018). Both the increasing number of *I. typographus* individuals and the species' range shift toward higher latitudes have led to increased stress and damage in forests (Lange et al., 2006). For instance, *I. typographus* has already caused vast forest damage in central Europe, especially as a secondary damage factor after large windthrows (Marini et al., 2017). The estimated frequency and damage of Northern European storms has increased, resulting in an increase in optimal reproduction material for *I. typographus* (Gardiner et al., 2010; Gregow et al., 2017; Marini et al., 2017). In Sweden, for instance, in 2005 and 2007, strong storms led to the colonization of approximately 1.4 million m^3 of Norway spruce; the unusually warm summer of 2018 then resulted in about1.5 million m^3 of bark-beetle-affected forest (Långström et al., 2009). The uncertainty in estimating how climate change affects both bark beetles' dynamics (among other disturbances) and the resulting forest decline is one of the largest sources of error in evaluations of forests' role in climate-change mitigation (Trumbore et al., 2015).

Early detection of damage by *I. typographus* is important for the mapping and mitigation of forest disturbances (Abdullah et al., 2019). Several researchers have investigated the estimation of *I. typographus*-induced forest damage using airborne sensors. The mapping of *I. typographus*-caused mortality using hyperspectral imagery can result in high overall accuracies (94%–97%) when a generic algorithm is used to select the spectral regions (Fassnacht et al., 2014). Depending on the type of algorithm, the selected bands can involve the red edge (680–690 nm), near-infrared (e.g. 1076 nm), or short-wave infrared (e.g. 1532, 1651, 2065, 2245, and 2280 nm). Hyperspectral imaging (517–814 nm) from an unmanned aerial vehicle shows potential for detecting infested trees, as it can produce a relatively good overall classification accuracy of 76%, with the largest differences in reflectance between infested and healthy trees in the near-infrared region around 750–814 nm (Näsi et al., 2015). By forecasting forest vitality with airborne hyperspectral imaging, researchers achieved an overall classification accuracy of 64% for healthy and infested forests, such that the best spectral characteristics for determining spruces' vitality status are located between 450 and 890 nm (Lausch et al., 2013). Early detection of the mountain-pine beetle (*Dendrotonus ponderosae* Hopkins) using hyperspectral data indicates that the strongest spectral features for detecting the green-attack stage (which occurs before there is visible deterioration of the canopy) are between 950 and 1390 nm (Cheng et al., 2010; Niemann et al., 2015). The effects of cell structure and LWC generally dominate the spectral responses of plants in this region. Scholars have also used the Sentinel-2 satellite to discriminate between healthy forests and *I. typographus* green-attacked areas with an overall accuracy of 67% (Abdullah et al., 2019). In that study, the largest spectral differences between healthy and infested foliage were in the following regions: 520–685 nm, 740–1130 nm, 1420–1850 nm, and 2000–2200 nm. Abdullah et al. (2018) were the first researchers to detect the green-attack stage of *I. typographus* infestation with fairly good accuracy, but their study area consisted of 30 m × 30 m plots that were fully under green attack from bark beetles. This situation rarely occurs in Nordic countries, where infestations are generally spatially dispersed and affected by local conditions (Blomqvist et al., 2018; Eriksson et al., 2007). Other researchers have mainly succeeded in mapping dead trees and forest areas with severe infestation symptoms; the existing remote-sensing methods have shown relatively good accuracy. Still, the early detection of *I. typographus* using remote sensing methods is challenging, especially if the infestation is dispersed and the crown symptoms are weak, as is typical in an early outbreak of *I. typographus* (Blomqvist et al., 2018).

Terrestrial lidar, or terrestrial laser scanning (TLS), can be used to accurately measure the 3D structures of forest environments, thus enabling the mapping of trees' functional traits (e.g., leaf area index) or forests' structural parameters with good accuracy (Liang et al., 2016; Zhu et al., 2018). In addition to this 3D information, TLS can measure the strength of backscattered light, which is referred to as *intensity*. This intensity can be described using the radar equation, which states that transmitted power (P_t), aperture area (D), optical efficiency (Q), laser-beam divergence (β), atmospheric transmission losses (T), range (R), and backscattering target cross-section (σ) all affect received power (P_r):

$$P_r = \frac{P_t D Q}{4\pi\beta^2} T^2 \frac{\sigma}{R^4}, \quad (1)$$

where σ comprises target reflectance, geometry, and illuminated area. According to Eq. (1), P_r is linearly dependent on transmitted power, aperture, optical efficiency, and target reflectance. Atmospheric transmission losses can be neglected in a terrestrial forest environment. However, the effect of R varies depending on the shape of the target (as a result of spherical losses). Variations in the powers of R can be observed between large planar surfaces that fill the entire laser footprint and linear or blob-like targets that partially cover the footprint (Wagner et al., 2006). Large surfaces create reflections that diminish less with distance than do reflections from wires or needles. Both incidence angle and the reflective properties of the target also influence intensity, which further complicates the calibration of that measure (Kaasalainen et al., 2011; Kaasalainen et al., 2018).

Many scholars have used TLS intensity to measure leaves' biochemical properties, including nitrogen, chlorophyll, and water content, but the radiometric calibration of this measure has been challenging (Eitel et al., 2014; Eitel et al., 2010; Eitel et al., 2011; Gaulton et al., 2013; Zhu et al., 2015). Traditionally, each TLS operates on a single-wavelength. However, recent developments in laser technologies have enabled dual-wavelength, multispectral, and even hyperspectral TLSs that simultaneously operate at multiple wavelengths, thus allowing for the measurement of forests' structural and spectral properties (Douglas et al., 2012; Hakala et al., 2012; Niu et al., 2015). Some researchers have used several TLSs to add wavelengths to these measurements (Elsherif et al., 2018; Junttila et al., 2018). Depending on the properties of a leaf's surface, using a spectral index from two wavelengths can reduce the effects that incidence angle and the various target cross-sections have on the measured value (Junttila et al., 2018; Kaasalainen et al., 2016).

Multispectral TLS has potential for the accurate mapping of LWC in controlled environments (Gaulton et al., 2013; Junttila et al., 2016). For instance, Junttila et al. (2018) used multispectral TLS to predict the LWC of Norway spruce (*P. abies* [L.] Karst.) seedlings, resulting in good agreement between LWC and spectral indices (coefficient of determination, $R^2 = 0.91$). However, thus far, researchers have only conducted studies in controlled environments that have with little variation in plant material or in environmental factors such as temperature and humidity. LWC, chlorophyll, and nitrogen concentration are significantly affected even in the green-attack stage of an *I. typographus* infestation (Abdullah et al., 2018, 2019). This stage is usually followed by discoloration of the crown (from green to yellow to reddish brown) and by defoliation (Coulson et al., 1985). Similarly, researchers have found significant differences in LWC during the green-attack stage of infestations involving the mountain-pine beetle (Cheng et al., 2010). Because the 1550 nm wavelength is sensitive to variance in LWC, multispectral TLS could be used to detect varying levels of bark-beetle infestation (Hunt Jr and Rock, 1989; Zhu et al., 2015). However, in

addition to the 1550 nm wavelength, a second wavelength in the near-infrared region is required to normalize the effects on a leaf's structure (both its internal structure and its dry matter); the 905 nm wavelength, which is not sensitive to LWC, is suitable for that purpose (Ceccato et al., 2001; Junttila et al., 2018; Peñuelas et al., 1997). Additionally, this wavelength could aid in detecting *I. typographus* infestations, as the near-infrared region is affected during the green-attack stage (Abdullah et al., 2019). Scholars have used TLS to detect defoliation due to the European pine sawfly (*Neodiprion sertifer* Geoffr.) by measuring the changes in lidar returns over time (Kaasalainen et al., 2010). However, the use of dual-wavelength lidar intensity metrics in the detection and assessment of bark-beetle infestation symptoms has not yet been studied.

The objective of this study was to investigate the potential value of dual-wavelength TLS in, first, detecting various symptoms of *I. typographus* infestation and varying LWC in a mature Norway spruce forest; and second, providing objective assessments of tree decline, with an emphasis on the exploitation of intensity information. TLS and other lidar point-cloud collection methods, such as mobile lidar systems and systems that use unmanned aerial vehicles, are increasingly being used whenever accurate forest-structure measurements are required. The development of lidar-based measurements of tree decline could allow for a single-sensor solution for the simultaneous and automatic measurement of forests' structures and trees' health (Eitel et al., 2016). To address the research questions raised above, two TLSs (operating at the 905 and 1550 nm wavelengths) were used to measure mature, *I. typographus*-infested Norway spruce trees. The infestation symptoms were classified in the field according to the severity of the crown and stem symptoms. The hypothesis was that infestation symptoms (e.g., discoloration, defoliation, and resin flow) significantly affect lidar intensity distributions, thus allowing for the detection of infested trees. The aims of the study were as follows: 1) to investigate the capability of multisensor dual-wavelength TLS in predicting various *I. typographus* infestation levels, with an emphasis on the early detection of *I. typographus* colonization; 2) to study the relationship between LWC and the level of *I. typographus* infestation; and 3) to examine dual-wavelength lidar's potential for estimating LWC in a mature Norway spruce forest.

2. Methods

2.1. Field measurements

The field measurements were conducted in August 2017 in the Viitalampi Forest, within the Ruokolahti municipality in southeast Finland (Fig. 1). The study area comprises a forest of mature Norway spruce mixed with European rowan (*Sorbus aucuparia* L.), European aspen (*Populus tremula* L.), and silver birch (*Betula pendula* Roth). The forest area suffered major damage from a 2010 storm and milder damage from subsequent storms, so it has provided a continuously optimal source for *I. typographus* breeding, leading to an elevated amount of related damage within the study area. In all, 33 Norway spruce trees were selected for further measurements according to their infestation status. The aim was to sample an even distribution of trees at various infestation levels. However, the cold summer of 2017 reduced the damage caused by *I. typographus*, so there were relatively few trees with severe symptoms in the study area; thus, the empirical data is characterized by low to moderate damage among the green-attacked trees (i.e., those that are colonized but that have no canopy discoloration). No dead trees were selected because the emphasis was on the early infestation symptoms.

The height of each tree and the height of its living crown were measured using a Vertex hypsometer (Haglöf Sweden AB, Långsele, Sweden); in addition, a caliper was used to measure diameter at breast height (DBH; Table 1). To measure each tree's LWC, needle samples were collected before midday (between 10:00 and 12:00) from two heights in the canopy: one from the upper third and one from the middle third. The samples were collected from the same side as the lidar measurement so as to ensure a match between the lidar and LWC data. The needle samples were taken by shooting down branches using a 12-gauge shotgun; the heights of the sample branches were recorded. Twigs of approximately 10 cm in length were cut from these branches, stored in zip-top bags, and placed in a cooler for transportation to the laboratory in order to prevent the loss of moisture. During the needle-sample collection, the temperature was approximately 12 °C, and the skies were overcast.

2.2. Assessment of symptoms and attack-level scores

Forest health experts visually assessed the symptoms caused by *I. typographus* for each tree in the field. The classification of these symptoms was based on visual assessments of the tree's crown and stem. The crown's color and foliage loss were assessed, as was the condition of the bark in terms of the number of resin-flow spots, the amount of bark's structural damage and the number of *I. typographus* entrance holes. Each symptom class was evaluated using a three-class scheme—*low* (1), *moderate* (2), and *high* (3)—except for the intensity of defoliation, which was assessed in four classes—0-25% (1), 25–50% (2), 50–75% (3), and 75–100% (4), following Blomqvist et al. (2018), who provided details on how the symptom classes are assessed in the field using this method.

A tree-wise attack-level score was developed using the classified symptoms. It was calculated as the sum of all the symptoms, thus forming a continuous variable of infestation intensity; for instance, a tree with green foliage and no defoliation, resin flow, entrance holes, or bark damage would get a score of 5. This attack-level score was then used to classify each tree into one of three classes: *no infestation* (score 5 or 6, $n = 10$), *low infestation* (score 7–11, $n = 13$), or *moderate infestation* (score 12–15, $n = 10$). The *low infestation* class included eight green-attacked trees that had been colonized but whose crowns lacked discoloration.

2.3. TLS measurements

Of the 33 sampled trees, 29 were measured using two TLSs of different wavelengths. The TLS instruments used were a FARO X330 (FARO Europe GmbH & Co. KG, Korntal-Münchingen, Germany), which operates at 1550 nm; and a Trimble TX5 (Trimble Inc., Sunnyvale, CA, USA), which operates at 905 nm. These scanners have similar technical specifications, and both utilize phase shifting range measurements (Table 2). Each tree was scanned from the same position with one scanner and then the other so as to avoid wind effects. The scanning distances varied from 7.5 m to 18 m, according to the terrain and the position of the trees. Both scanners' resolutions were set to 0.25, resulting in a vertical spacing of 6.14 mm at a 10 m distance; the quality parameter was set to 2× (i.e., two measurements were made for each point, and the resulting value was the mean of the two). The scanners have same beam divergence (0.19 mrad), resulting in 6.1 mm and 6.8 mm laser-beam diameters at 10 m for the FARO X330 and Trimble TX5, respectively. Four target spheres (each of diameter 140 mm) were placed around the scanner for further scan registration. A Lambertian Spectralon reflectance panel (Labsphere, North Sutton, NH, USA) with a nominal reflectance of 20% was used as a reference target to normalize the laser intensity. The temperature during data acquisition was approximately 13 °C, the relative humidity was approximately 60%, and the wind speed varied from 3 to 4 m/s.

Additional TLS measurements were conducted in a laboratory setting to evaluate the sensitivity of the lidar intensity to varying incidence angles and distances. Spectralon reflectance panels with nominal reflectance of 99% and 40%, as well as silver birch and Norway maple (*Acer platanoides* L.) leaves, were measured at incidence-angle intervals of 10° from 0° to 70°. The 40% reflectance panel was also measured at 2-m intervals to determine the relationship between intensity and

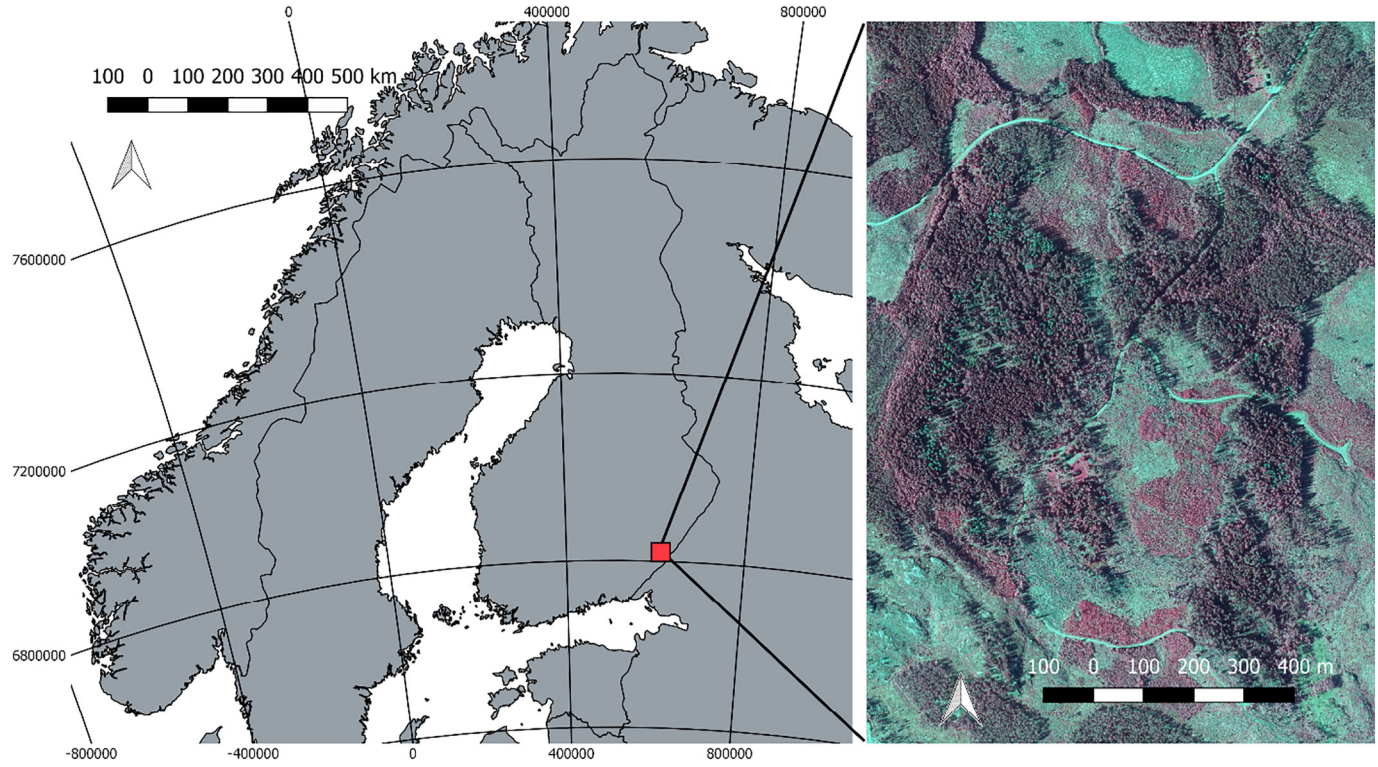

Fig. 1. A map of the Viitalampi study-area location and an aerial false color image of the study area (near-infrared values are shown in red; red values are shown in green; and green values are shown in blue). (For interpretation of the references to color in this figure legend, the reader is referred to the web version of this article.)

Table 1
Summary statistics for tree structure, attack-level score, and several leaf measures.

Variable	Mean	Std. dev.	Min.	Max.
DBH (cm)	29.0	6.69	18.9	55.4
Height (m)	25.2	2.81	18.8	30.3
Attack-level score	9.4	3.00	5	15
Equivalent water thickness (g/cm^2)	0.013	0.0061	0.0037	0.031
Gravimetric water content (%)	54.1	3.58	45.3	60.4
Leaf mass per area (g/cm^2)	0.011	0.0054	0.0028	0.024

distance.

2.4. LWC measurements

Approximately 30 needles were randomly collected from among the sample twigs in the laboratory. The fresh weight of these needles was weighed (with a precision of 0.0001 g), their combined leaf area was scanned using an Epson V370 Photo flatbed scanner (Epson America, Inc., San Jose, CA, USA) at 800-dpi resolution, and the samples were dried in an oven at 60 °C for 48 h before their dry weight was measured. The scanned images were analyzed using the R software package so as to calculate leaf area by segmenting the needles in the images and transforming the number of segmented pixels into a leaf-area value based on the scanner's resolution (R Core Team, 2013). This calculated leaf area was multiplied by 2.57 to take into account the pyramidal shape of the needles and then divided by 2, resulting in a one-sided leaf area (Waring, 1983). LWC was then calculated as both equivalent water thickness (EWT; Danson et al. (1992)) and gravimetric water content (GWC; (Datt, 1999)), as follows:

$$EWT = \frac{FW - DW}{A}\left(\frac{g}{cm^2}\right), \quad (2)$$

$$GWC = \frac{FW - DW}{FW}\left(\frac{g}{g}\right), \quad (3)$$

where FW (g) is the fresh weight, DW (g) is the dry weight, and A (cm^2) is the leaf area of the fresh sample.

2.5. The processing of TLS data

The subsequent TLS scans at both wavelengths were registered to a common (arbitrary) coordinate system using FARO Scene software. The four sphere targets were used to align the point clouds using the Helmert transformation process (Watson, 2006), resulting in a mean accuracy of 4.5 mm between targets. Each tree was manually segmented from the point clouds using the CloudCompare software package (version 2.10) for further processing (Girardeau-Montaut, 2011). Because the laser scanners utilize the phase-shifting technique for range measurements, a large amount of noise (e.g., ghost points) was apparent in the point clouds (Balduzzi et al., 2011). To reduce the number of ghost points, a statistical-outlier algorithm was applied to the point clouds in order to filter out the points that are far from other

Table 2
Technical specifications of the laser scanners.

Laser scanner	Beam divergence (mrad)	Beam diameter at exit (mm)	Wavelength (nm)	Output power (mW)	Scan rate (kHz)	Intensity recording (digital number)	Ranging error (mm)
FARO X330	0.19	2.25	1550	500	488	−2048 to 2033	± 2
Trimble TX5	0.19	3	905	20	488	−2048 to 2033	± 2

points (based on the distance to the neighboring points). The maximum distance for a point to be included was calculated as follows:

$$MaxD = MeanD + nSigma \times Std.\ Dev.\ , \quad (4)$$

where *MaxD* is the maximum distance for a point to be included, *MeanD* is the mean distance to the neighboring points, *nSigma* is the standard-deviation multiplier threshold, and *Std. Dev.* is the standard deviation of the distance of the neighboring points. The algorithm parameters were determined based on a visual examination of the resulting point cloud. For each point cloud, the number of neighbors was set to 8, and *nSigma* was set to 0.7.

Classification of the needles and stem points was required to investigate how the lidar intensity responds to varying LWC values. However, as the spruce needles were smaller than the laser footprint, the twigs and needles could be illuminated simultaneously, making it impossible to separate true needle points from points that are a mix of needles and twigs or branches. Thus, the classification instead was based on the separation of tree stems and twigs from needles. This classification was done using a classifier based on the multiscale dimensionality criterion (Brodu and Lague, 2012); the system was trained with 40,000 manually classified needle and stem points from eight trees. The reported balanced accuracy of the training sample was 0.95. The classifier was then applied using the CloudCompare software package. The classification procedure provided the confidence level of the classification as an output; only points with a confidence value of at least 0.98 were used.

2.6. Intensity calibration

The calibration of intensity was necessary due to the variety of factors that affected the measured intensity. The data-processing workflow, which included distance and logarithmic corrections and the normalization of intensity, is illustrated in Fig. 2. Lidar intensity is sensitive to range, so a range correction is required (Kaasalainen et al., 2011). The relationship between range and lidar intensity was investigated by scanning a Spectralon panel with a nominal reflectance of 40% at 2-m intervals from 3 m to 33 m. Distance strongly affected the intensity of both scanners—especially distances of < 20 m, where the intensity showed a peak, followed by a positive slope toward longer distances (Fig. 3).

For the reflectance panel polynomial, the model was fitted to the acquired empirical relationship between range and mean intensity, similar to the approach of Tan et al. (2016). This approach was improved using an external reference target to normalize the intensity; this allowed for the removal of the effect of varying instrument temperatures (Errington and Daku, 2017). This model was then used to remove the effect of the distance from each point cloud on the raw laser intensity, using a polynomial model of degree 10 within R (version 3.4.3, (R Core Team, 2013)), as shown in Table 3. The variation of intensity caused by changes in distance was significantly reduced after the distance correction, with the test data set having just 5.9% and 3.4% of the original variation for the X330 and TX5 scanners, respectively.

Both TLSs have showed logarithmic relationship between intensity and reflectance, especially for low-reflectance targets (Junttila et al., 2018; Kaasalainen et al., 2009). Thus, the distance-corrected intensity was transformed into a relative reflectance using an empirical model based on scans of the Spectralon reflectance panels at nominal reflectance values of 5%, 10%, 20%, 40%, and 60%. This logarithmic correction was done using the following equation (Kaasalainen et al., 2009):

$$y = 10^{\frac{(x-A_1)}{A_0}}, \quad (5)$$

where A_0 and A_1 are empirical parameters determined by fitting the measured intensity and reflectance of the reflectance panels (Fig. 4). The model parameters, A_0 and A_1, were 503.9 and 1758.7 for the Trimble TX5 and 438.9 and 2020.5 for the FARO X330.

Finally, the distance and log corrected intensity were normalized with the mean intensity of an external reference target (a Spectralon panel with 20% nominal reflectance) to eliminate any effects on the intensity due to a varying instrument or ambient temperature. The output of the intensity-calibration process is referred to as *calibrated intensity* within this paper. Incidence angle was not considered during the calibration procedure due to the small sizes of the needles, which resulted in multiple scattering when the laser-beam diameter at the target was larger than the width of a single needle. This complicated the calculation of the incidence angle from the point cloud but should not have caused large errors, as (based on a previous study of lidar intensity), the Norway spruce is less affected by incidence angle than deciduous species are (Kaasalainen et al., 2018).

A normalized difference index (NDI) was calculated for each point by finding the nearest neighbor in the point clouds for the 905 and 1550 nm wavelengths, using the following equation:

$$NDI = \frac{I_{905} - I_{1550}}{I_{905} + I_{1550}}, \quad (6)$$

where I is calibrated intensity at the wavelength indicated by the footnote. A maximum distance of 1 cm was used to filter the points and to ensure geometrical similarity between the point clouds.

2.7. Explanatory variables

A set of intensity metrics was calculated for each point cloud (Table 4). These metrics are based on statistics that describe the distribution of intensity values within a given point cloud. The metrics were individually calculated for the 905 and 1550 nm wavelengths and for the NDI. These metrics were calculated separately and at the tree level for classified needle points in the canopy and for stem points between 1.6 m and 3.6 m in height. Because the upper parts of the stems could not be visually assessed, a height range was used. The utilization of two independent point clouds for each tree enabled the development of more complex regression models. The subscript indicates the source of the calculated metric, and i denotes the wavelength or NDI (e.g., 1550_mean_{canopy}).

2.8. Statistical analysis

The differences in GWC and EWT between the various infestation classes were assessed using two-sided, independent-sample Student's *t*-tests. Each group was tested for normality using the Shapiro-Wilk test (Royston, 1982). If non-normality was detected, the Kolmogorov–Smirnov test was used instead of a *t*-test. The correlations between infestation symptoms and both LWC metrics and tree structural attributes were assessed using Pearson correlations for the continuous variables and using Spearman correlations when ordinal-scale variables were involved (i.e., for individual infestation symptoms).

Due to the ordinal nature of the assessed tree symptoms, ordinal logistic regression modeling was used to determine which intensity metrics provided the strongest links to the tree symptoms that could affect the lidar intensity distribution: resin flow, discoloration, and defoliation. This was done by producing cumulative link models with a single predictor and then comparing the models in terms of statistical significance and McFadden pseudo R^2 to determine the best predictors, using the following equation (Agresti, 2002; Agresti and Tarantola, 2018; McFadden, 1973):

$$R^2 = \frac{d0 - d}{d0}, \quad (7)$$

where *d0* is the deviance of a null model, and *d* is the deviance of the actual model. The McFadden pseudo R^2 describes how the deviance decreases compared to the null model. For each symptom, the six strongest predictors according to R^2 are reported in the Results section.

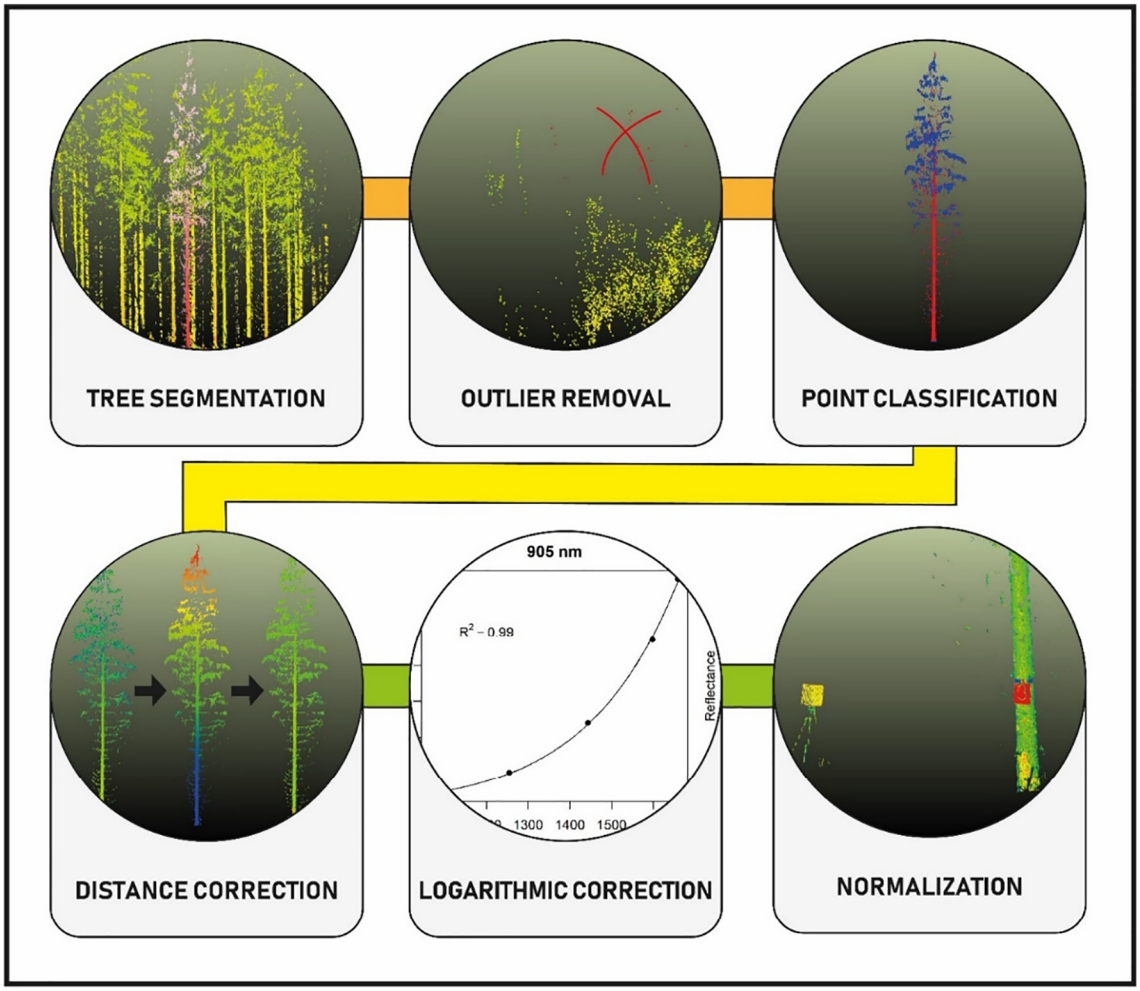

Fig. 2. The point-cloud processing workflow: tree segmentation, outlier removal, point classification, and then intensity calibration.

Linear-regression modeling was used to estimate each individual-intensity metric's ability to explain attack-level score, GWC, and EWT. A model was developed with each intensity metric as a predictor, and all the models were compared according to R^2 and root mean square error (*RMSE*). The six strongest predictors were reported.

Additionally, multiple-regression models were developed to evaluate the intensity metrics' ability to estimate attack-level score, GWC, and EWT. The regression models were developed using a sequential stepwise algorithm with a maximum of three explanatory variables, resulting in nearly 10 subjects per variable at the maximum number of variables ($n = 29$). At least two subjects are needed for each variable to ensure the reliable estimation of regression coefficients (Austin and Steyerberg, 2015). The Schwarz–Bayesian information criterion, which penalizes for model complexity, was used to select the model (Schwarz, 1978). Variance inflation factor was used to detect multicollinearity, and a simpler model was selected if this value was > 3 for a given variable (Zuur et al., 2010). Adjusted R^2 and predicted R^2 were used to evaluate the goodness of fit so as to avoid overfitting the models. The accuracy of the developed regression models was assessed using *RMSE* and the coefficient of determination, which were calculated using leave-one-out cross-validation, per the following equations:

$$RMSE = \sqrt{\frac{\sum_{i=1}^{n} (y_i - \hat{y}_i)^2}{n}}, \quad (8)$$

$$RMSE\% = 100 \times \frac{RMSE}{y_{max} - y_{min}}, \quad (9)$$

where n is the number of observations, y_i is the observed value for the measurement i, $\hat{y}_i$ is the predicted value for the measurement i, y_{min} is the minimum of the observed data, and y_{max} is the maximum of the observed data.

To assess the separability between the infestation classes, linear discriminant analysis (LDA) was conducted using the "mass" package in R (Ripley et al., 2013). Two classification schemes were tested: a three-class scheme (*no infestation*, *low infestation*, and *moderate infestation*) and a two-class scheme (*not infested* and *infested*). The number of explanatory variables in the LDA was kept to the maximum of three, and the variables were chosen based on the results of the ordinal logistic regression so as to avoid overfitting due to the limited number of samples ($n = 29$). The accuracy of the classification was then computed using leave-one-out cross-validation. All of the statistical analyses were conducted in R (version 3.4.3, (R Core Team, 2013)).

3. Results

3.1. The relationship between I. typographus symptoms and LWC

Among the LWC metrics, only GWC is affected by the symptoms of *I. typographus* infestation (Fig. 5). GWC shows a significant correlation ($p < 0.001$) with attack-level score and is significantly correlated with all infestation symptoms except for bark damage (Table 5). GWC shows the strongest correlation with discoloration of the crown. GWC is significantly lower for trees in the *medium infestation* class than those in the *low infestation* class, which in turn is significantly lower than in the *no*

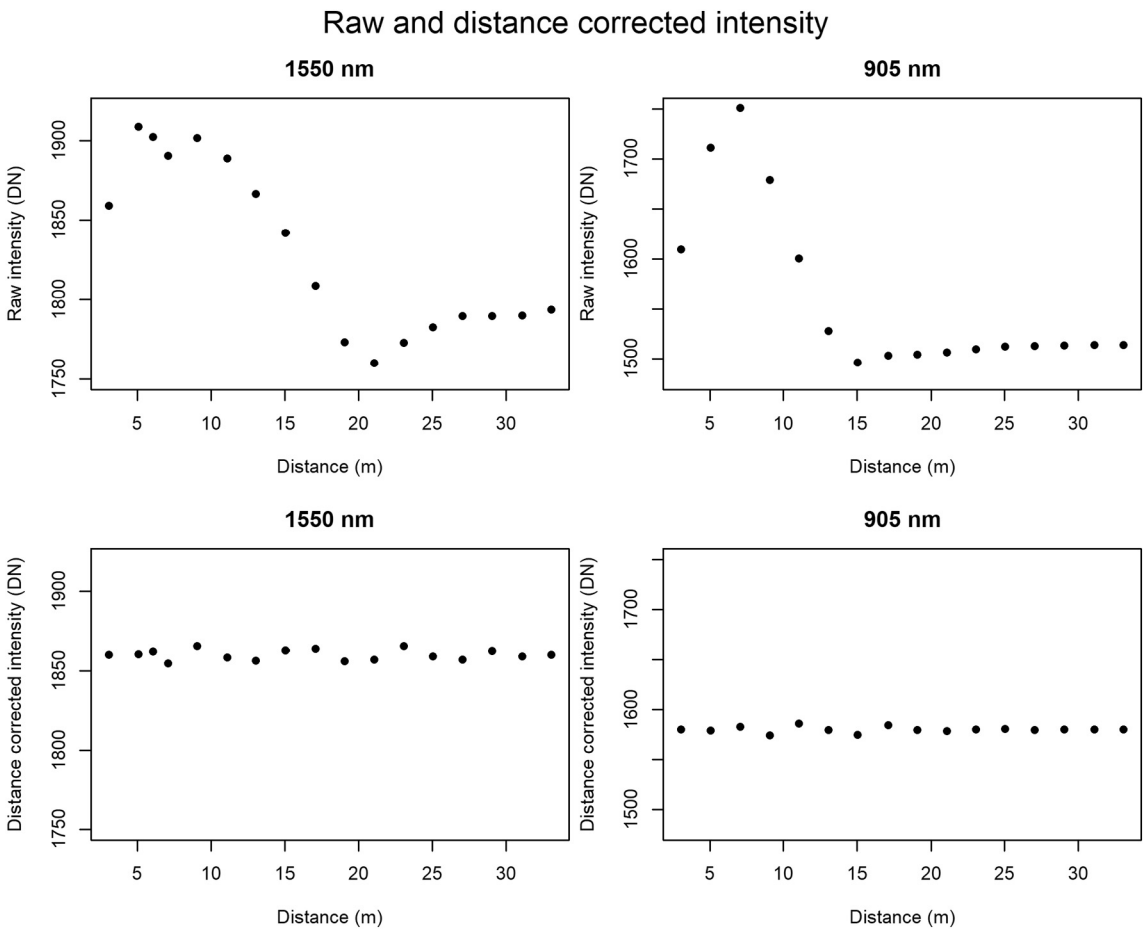

Fig. 3. The relationship between raw intensity and distance, before and after the distance correction.

Table 3
The polynomial model parameters used for the distance correction of lidar intensity.

Parameter	Trimble TX5	FARO X330
Intercept	1826.5	1550.813
a_1	−142.5	−214.561
a_2	126.0	167.473
a_3	0.3037	−58.98
a_4	−75.7555	−54.93
a_5	65.4323	121.396
a_6	−1.75	−112.53
a_7	−19.41	51.282
a_8	8.4852	1.697
a_9	26.2545	−32.113
a_{10}	−21.18	25.183

infestation class ($p < 0.05$). Due to non-normality in the *no infestation* class of EWT, the Kolmogorov–Smirnov test was used to compare the *no infestation* and *low infestation* classes of EWT. However, no significant changes between the infestation classes exist, and no significant correlation exists between EWT and attack-level score.

3.2. Other factors that affect LWC

EWT shows a strong correlation with leaf mass area (LMA), a measure of leaf density ($r = 0.93$), but not with GWC (Table 5). Sampling height shows a significant correlation with EWT: higher sample heights correlate with higher EWT. LMA also correlates positively with sampling height. In addition, GWC shows a weak but nonsignificant positive correlation with sampling height; thus, LWC seems to exhibit vertical variation within the tree crown.

3.3. Sensitivity of lidar intensity to varying incidence angles

Both wavelengths are sensitive to variations in the incidence angle (Fig. 6). The 99% reflectance panel shows a continuous decrease as the incidence angle increased; at the 70° angle, this results in an intensity reduction of 66.3% and 72.1% for the 905 and 1550 nm wavelengths, respectively. The NDI value stays near 0 for values up to 50°, at which point it increases slightly with increasing angles, up to 70°. The 40% reflectance panel shows a similar trend, with 60.8% and 70.2% decreases for the 905 and 1550 nm wavelengths at the 70° angle; the NDI also shows a slightly increasing trend, albeit with less volatility. However, the leaf samples for the silver birch and Norway maple have a different pattern, with a more linear decrease as the incidence angle increases. For the silver birch leaf samples, the 905 and 1550 nm wavelengths decrease by 66.0% and 78.3%, respectively; the NDI value increase by 72.5%. The Norway maple leaf samples show a smaller decrease in calibrated intensity: 57.5% and 68.8% for the 905 and 1550 nm wavelengths, respectively; the NDI value increases by 42.4%.

3.4. Lidar intensity response to infestation symptoms

The lidar intensity metrics for the 905 and 1550 nm wavelengths, as well as the calculated NDI, vary according to the infestation symptoms (Table 6). The extent of resin flow is best detected with the 905_range$_{stem}$, 905_max$_{stem}$, 1550_max$_{stem}$, and 1550_range$_{stem}$ features, thus indicating an increase in the strength of intensity due to resin on tree stem. Discoloration affects the following features most strongly: NDI_kur$_{canopy}$, 1550_p40$_{canopy}$, 1550_p30$_{canopy}$, 1550_p50$_{canopy}$, and

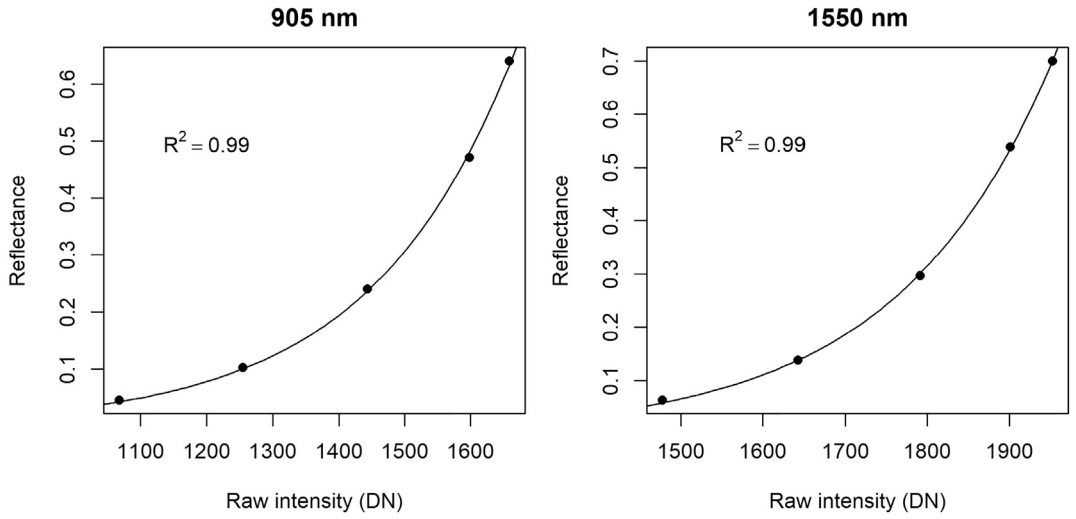

Fig. 4. The relationship between measured raw intensity (Digital Number, DN) and reflectance for both scanners, including the predicted reflectance that was used for correcting the logarithmic behavior.

Table 4
Summary of the calculated intensity metrics. N.B. *i* denotes the wavelengths 905 and 1550 nm, as well as the calculated NDI.

Metric	Description
*i*_mean	Average intensity
*i*_std	Standard deviation of intensity
*i*_p10, *i*_p20, … *i*_p90	Multiple-of-10 percentiles (10th through 90th) of the intensity distribution
*i*_max	Maximum intensity
*i*_min	Minimum intensity
*i*_kur	Kurtosis of the intensity distribution (Davies, 1947)
*i*_ske	Skewness of the intensity distribution (Davies, 1947)
*i*_entropy	Shannon diversity index (entropy) of the intensity distribution (Shannon, 2001)
*i*_MAD	Median absolute deviation of intensity (Leys et al., 2013)
*i*_range	Difference between maximum and minimum intensity
*i*_DBW	Density bandwidth calculated with the rule of thumb in the kernel density estimation (Silverman, 2018)
*i*_D05, *i*_D25, *i*_D50, *i*_D75	Density variables: the 95th percentile divided by 5th, 25th, 50th, and 75th percentiles, respectively.

905_ske$_{canopy}$. The intensity features that are most sensitive to defoliation are 1550_ske$_{canopy}$, 1550_max$_{canopy}$, 905_ske$_{canopy}$, and 1550_range$_{canopy}$. The features 905_ske$_{canopy}$ and 1550_ske$_{canopy}$ are among the top predictors of both discoloration and defoliation in the canopy. The 905_ske$_{canopy}$ feature also has the strongest explanatory power for the *infestation* class in the two-class system. Other predictors that are among the strongest predictors of this class include 1550_max$_{canopy}$, 1550_range$_{canopy}$, and NDI_kur$_{stem}$.

3.5. The prediction of infestation level and LWC

The results of the linear-regression models with single intensity metrics as predictors indicate that, at both wavelengths, the strongest predictor for attack-level score was skewness (905_ske$_{canopy}$ and 1550_ske$_{canopy}$), as shown in Table 7. Regarding GWC, the distribution of NDI from the stem has the strongest explanatory power; the canopy metrics show only weak correlations with GWC. The best predictors of EWT use the kurtosis of the 905 and 1550 nm wavelengths for the whole data set. The removal of a single outlier from the EWT data results in different intensity metrics (minimum, maximum, and range of NDI) that show the best explanatory power; removing the outlier also leads to slightly improved *RMSE*.

The developed multiple-regression models show fair agreement between the point-cloud and tree-infestation metrics (Fig. 7). The point-cloud metrics explain 50% of the variation in attack-level score (*RMSE* = 1.95), using intensity metrics from both the stem and the canopy (Table 8). The regression model for EWT shows slightly higher

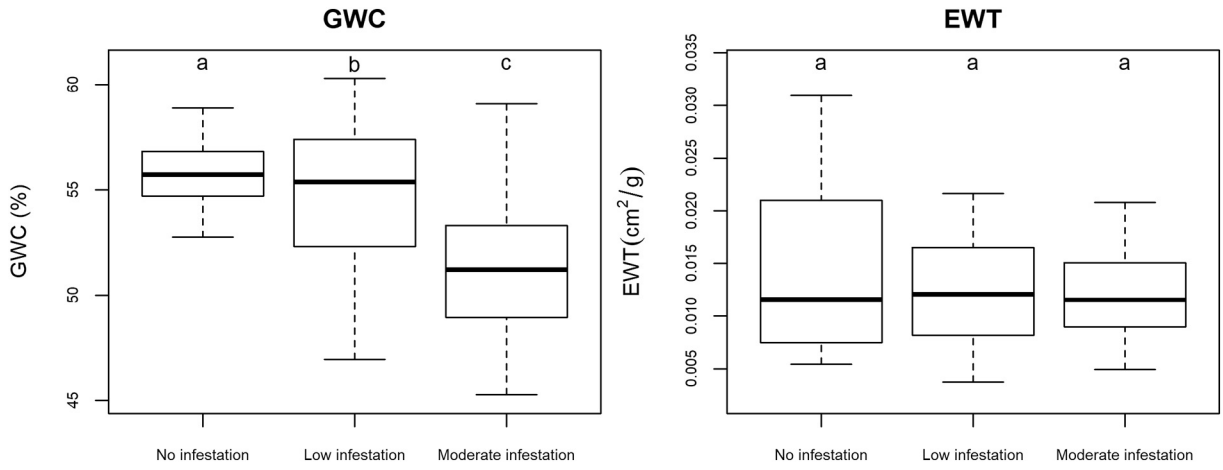

Fig. 5. Box plots of gravimetric water content (GWC) and equivalent water thickness (EWT) for the trees (n = 66) in each infestation class. There are significant differences ($p < 0.05$) between the a, b, and c groups.

Table 5
Correlation matrix of the infestation symptoms, attack-level score, structural attributes, and LWC (tree level, $n = 33$), as well as needle measurements (EWT, GWC, and sampling height) (twig level, $n = 66$). The correlations in bold are significant ($p < 0.05$).

	Attack-level score	Defoliation	Discoloration	Resin flows	Insertion holes	Bark damage	DBH	Tree height	Sampling height	EWT	GWC
LMA	−0.04	0.11	0.16	−0.10	−0.03	−0.28	0.21	0.20	**0.30**	**0.93**	−0.20
Attack-level score		**0.77**	**0.68**	**0.89**	**0.88**	**0.59**	−0.24	−0.14	–	−0.26	**−0.59**
Defoliation			**0.63**	**0.56**	**0.59**	0.09	−0.15	−0.07	–	−0.09	**−0.51**
Discoloration				**0.44**	**0.50**	0.19	0.08	−0.07	–	−0.05	**−0.71**
Resin flows					**0.89**	**0.57**	−0.04	−0.02	–	−0.12	**−0.39**
Insertion holes						**0.48**	−0.11	−0.03	–	−0.10	**−0.43**
Bark damage							−0.14	−0.13	–	−0.23	−0.14
DBH								**0.62**	–	0.19	−0.08
Tree height									–	0.15	−0.07
Sampling height										**0.34**	0.16
EWT											0.15

agreement between predicted and observed values (adjusted $R^2 = 0.68$, $RMSE = 0.0026$ g/cm^2); 48% of the variation in GWC ($RMSE = 2.03$) can be explained with a regression model that includes only stem-based intensity metrics. The canopy-based intensity metrics show low predictive power (adjusted $R^2 = 0.19$, $RMSE = 2.58$) for GWC. The removal of a single outlier from the EWT distribution results in slightly different explanatory variables; according to the stepwise algorithm, the mean and minimum canopy NDI are most appropriate. All the models employed a mix of intensity metrics from the 905 and 1550 nm wavelengths.

The explanatory variables selected in the models do not exhibit a clear trend, but similar intensity metrics are among the top predictors in the simple models. The models all include variety of intensity metrics from both the 905 and 1550 nm wavelengths and from the NDI. However, the presence of variables that explain the shape of the intensity distribution (e.g., skewness, kurtosis, and density) is pronounced in these models. Every model includes at least one explanatory variable that describes the shape of the distribution.

The LDA shows fair discrimination between the *not infested* and *infested* classes (Table 9), but the *low* and *moderate infestation* classes show weak accuracy. The overall accuracy is 66% in the three-class scheme but 90% in the two-class scheme. The classification accuracy is the same for *not infested* and *infested* trees in the two-class classification scheme, with a producer's accuracy of 75%.

4. Discussion

4.1. Incidence angle and distance effects on lidar intensity

The sensitivity of TLS intensity to varying incidence angles and calculated NDIs was studied to evaluate the extent to which NDI moderates the effect of the incidence angle. The results show that, with Lambertian scatterers such as the reflectance panels used in this study, NDI cancels out a large portion of the incidence angle's effect; the NDI value shows only a slight increase as incidence angles increase. However, the results of tests with leaf samples from fresh Norway maple and silver birch trees reveal that incidence angle influences the NDI nearly as much as it does the individual wavelengths. The NDI increases steadily with increasing incidence angles in both samples. This is likely due to the leaves' specular (mirror-like) reflection behavior, which results in differing relationships between intensity and incidence angle at each wavelength (Kaasalainen et al., 2018). NDI's incidence-angle dependency seems species-specific, as scholars have identified various types of relationships between NDI (and other spectral ratios) and incidence angle (Elsherif et al., 2018; Kaasalainen et al., 2016). Variations in wavelength affect Norway spruce less than they affect deciduous species (Kaasalainen et al., 2018). Tests are required to determine which leaf structures enable more reliable intensity measurements by reducing the incidence-angle effect. Conifer needles can exhibit a variety of incidence angles, even within a single lidar footprint, which complicates corrections for incidence angle. Moreover, the varying cross-section of lidar-illuminated needles creates additional variations in the intensity measurements. However, scholars have recently shown that NDI can reduce these effects among coniferous species, as compared to single-wavelength intensity (Junttila et al., 2016, 2018).

The intensity response of Norway spruce among other conifer species is characterized by a so called edge effect, in which the target does not completely fill the laser beam's diameter, resulting in a weaker intensity response (Eitel et al., 2010). Fig. 8 shows how, in each defoliation scenario, the laser footprint encounters a distinct amount of target edge, as well as how the complexity of the surface pattern varies under the illuminated area. The effect that distance has on the reflected light (and therefore on the measured intensity) can explain the reduction in the strength of the intensity response. The range has at least double the effect on small linear targets as it has on large surfaces (Korpela, 2017). Well-defined surfaces thus show much higher intensities than complex surfaces (e.g., needles or branches with needles), which was observed in the data for this study as well. Although the reflectance of needles and bark should be near the same magnitude (Hoque et al., 1990), bark has nearly twofold higher calibrated intensity than foliage. Similarly, the skewness values of both the 905 and 1550 nm wavelengths are among the strongest predictors for defoliation in this study despite the low intensity of defoliation observed in the data; this indicates that a reduced amount of edge in the defoliated canopies influences the intensity-value distribution. Therefore, the absolute calibration of lidar intensity is complicated by the effect of the varying target distance within the canopy. This distance correction should be further investigated using other coniferous tree species so as to improve the radiometric calibration of TLS intensity. According to this study's results, the lidar-intensity distribution can explain part of the variation in infestation severity despite these challenges.

4.2. LWC as an indicator of bark-beetle infestation

The measured LWC from Norway spruce trees with varying *I. typographus* infestation levels shows that LWC varies due to the rate of bark-beetle colonization. Significant differences in GWC exist between the *no infestation* and *low infestation* groups, despite the relatively small sample size of 33 trees. The relationship between GWC and infestation severity is linear, even though the study area is entirely characterized by *low* and *moderate infestation* symptoms due to the low temperatures and high precipitation during the summer of the sample collection. GWC shows significant correlations with all the observed infestation symptoms except for bark damage, but the strongest is the discoloration of the crown, which has a correlation coefficient of 0.71. Infestation severity does not significantly affect EWT; however, EWT has a weak negative trend with increasing bark-beetle infestation severity. Other researchers have identified a significant decrease in EWT in the upper canopy during the green-attack stage of infestation (Abdullah et al.,

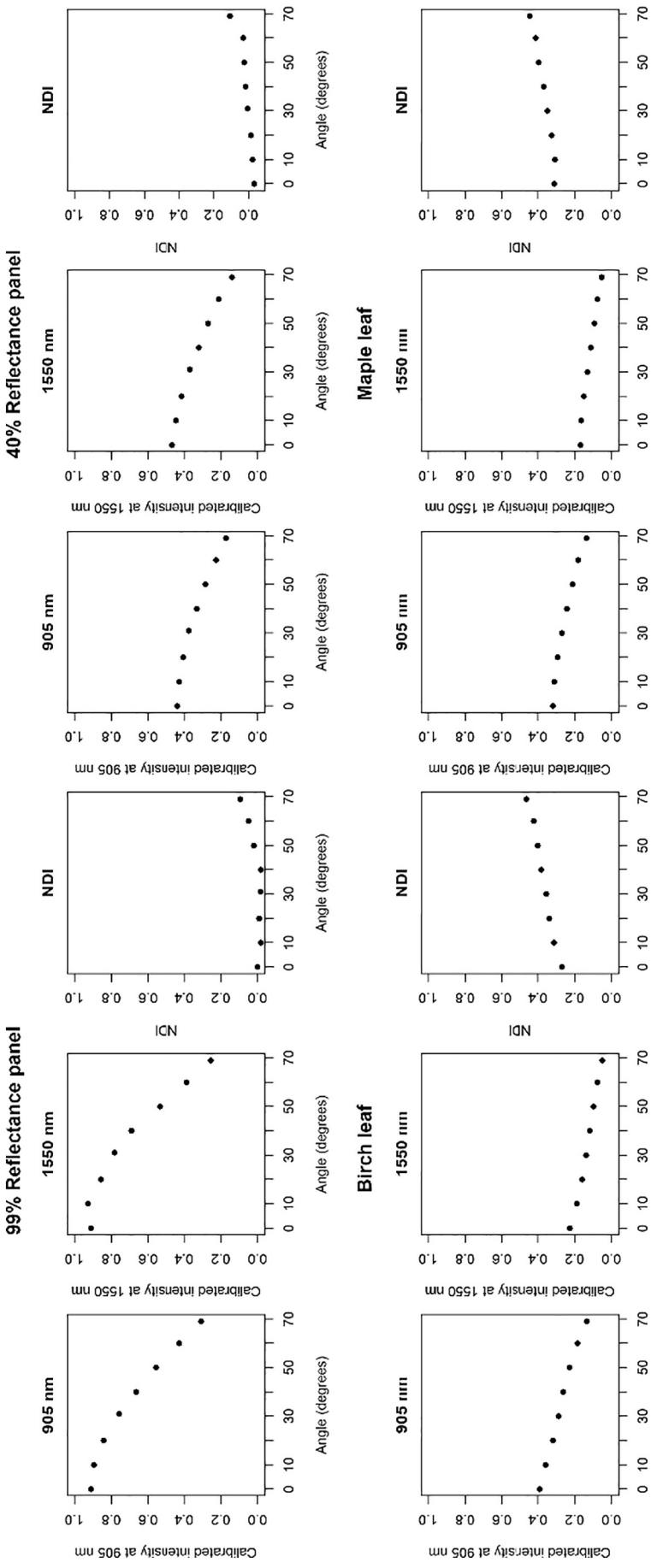

Fig. 6. The relationship between calibrated intensity and incidence angle at the 905 and 1550 nm wavelengths, as well as the calculated NDI using the following targets: 99% and 40% nominal reflectance panels, silver birch leaves, and Norway maple leaves.

Table 6
Summary of the statistics for the ordinal logistic-regression models for infestation symptoms, infestation class, and the individual-intensity metrics. The six strongest predictors for each symptom are reported here.

Resin flow			Discoloration		
Intensity metric	p	R^2	Intensity metric	p	R^2
905_range$_{stem}$	0.034	0.14	NDI_kur$_{canopy}$	0.024	0.23
905_max$_{stem}$	0.043	0.12	1550_p40$_{canopy}$	0.011	0.20
1550_max$_{stem}$	0.057	0.10	1550_p30$_{canopy}$	0.0085	0.19
1550_range$_{stem}$	0.056	0.10	1550_p50$_{canopy}$	0.013	0.19
905_ske$_{stem}$	0.037	0.09	905_ske$_{canopy}$	0.012	0.19
NDI_D75$_{stem}$	0.086	0.05	1550_ske$_{canopy}$	0.010	0.18

Defoliation			Infestation class		
Intensity metric	p	R^2	Intensity metric	p	R^2
1550_ske$_{canopy}$	0.0068	0.13	905_ske$_{canopy}$	0.0025	0.20
1550_max$_{canopy}$	0.011	0.11	1550_max$_{canopy}$	0.0053	0.19
905_ske$_{canopy}$	0.0096	0.11	1550_range$_{canopy}$	0.0059	0.18
1550_range$_{canopy}$	0.013	0.11	NDI_kur$_{stem}$	0.0071	0.14
905_p60$_{canopy}$	0.011	0.10	NDI_D50$_{stem}$	0.0095	0.13
905_p50$_{canopy}$	0.012	0.10	NDI_D25$_{stem}$	0.0098	0.13

2019), as well as significant reflectance differences in the water absorption bands within the canopy (Immitzer and Atzberger, 2014). Within-tree variation and relatively small sample sizes may have hindered the detection of significant EWT differences in this study.

There is a strong relationship between EWT and LMA in this study ($r = 0.93$). Both measures express significant, positive correlations with sampling height and seem to vary due to local illumination. Scholars have found similar vertical variations of EWT before, but only with smaller trees (Elsherif et al., 2018). Local illuminance conditions affect LMA due to its relationship between photosynthetic capacity, which is supported by the correlation between sample height and LMA (Poorter et al., 2009). These results suggest that GWC is a more robust indicator of leaf water status than EWT.

4.3. Predicting LWC with lidar intensity

The linear-regression models for GWC and the individual-intensity metrics reveal a relationship with an R^2 of 0.38 (*RMSE* = 2.35) between NDI_p10$_{stem}$ metric and GWC. The higher percentiles and the NDI_mean$_{stem}$ have similar relationships. A multiple-regression model with three intensity metrics (NDI_kur$_{stem}$, 1550_D75$_{stem}$, 1550_p40$_{stem}$) from the stem explained 48% of the variation in GWC (*RMSE* = 2.03). Scholars have used NDI to estimate EWT, which is sensitive to water content (Gaulton et al., 2013; Junttila et al., 2018), so NDI could also possibly be used to measure bark water content and to indicate a tree's water status. There could be a link between GWC and bark water content because bark beetles feed on phloem, ultimately causing trees to die, dry out, and drop their bark. Bark water content is sensitive to moisture stress, which can increase a tree's susceptibility to bark-beetle attacks (Lorio Jr and Hodges, 1968; Økland and Berryman, 2004). No measurements of bark water content were conducted in this study, so this remains speculative. However, the consistency and the strength of the relationship between stem NDI and GWC is an unexpected outcome that is worth investigating in future studies so as to further evaluate the potential value of stem lidar intensity measurements.

The canopy-intensity metrics show the capability of explaining EWT (adjusted $R^2 = 0.68$, *RMSE* = 0.0026 g/cm^2), but the accuracy may be overestimated due to a single EWT value that is significantly higher than the rest of the data points. The developed regression models for EWT show that the NDI and 1550 nm wavelength features are among the best predictors for EWT, which is in line with what researchers have found in previous studies in which they estimated the effectiveness of

Table 7
Summary of the six strongest individual-intensity predictors of the linear-regression models for attack-level score, GWC, and EWT.

Attack-level score				GWC			
Intensity metric	R^2	*RMSE*	*RMSE*%	Intensity metric	R^2	*RMSE*	*RMSE*%
905_ske$_{canopy}$	0.39	2.28	22.8	NDI_p10$_{stem}$	0.38	2.35	22.1
1550_ske$_{canopy}$	0.30	2.45	24.5	NDI_p20$_{stem}$	0.37	2.37	22.3
1550_max$_{canopy}$	0.27	2.49	24.5	NDI_p30$_{stem}$	0.36	2.39	22.4
1550_range$_{canopy}$	0.26	2.51	25.1	NDI_p40$_{stem}$	0.35	2.41	22.6
905_p30$_{canopy}$	0.24	2.55	25.5	NDI_mean$_{stem}$	0.34	2.42	22.8
905_p20$_{canopy}$	0.23	2.55	25.5	NDI_p50$_{stem}$	0.34	2.43	22.8

EWT				EWT (without outliers)			
Intensity metric	R^2	*RMSE*	*RMSE*%	Intensity metric	R^2	*RMSE*	*RMSE*%
905_kur$_{canopy}$	0.33	0.0039	16.3	NDI_min$_{canopy}$	0.16	0.0033	26.8
1550_kur$_{canopy}$	0.33	0.0040	16.4	NDI_range$_{canopy}$	0.16	0.0033	27.0
1550_ske$_{canopy}$	0.32	0.0040	16.5	NDI_max$_{canopy}$	0.15	0.0033	27.0
1550_range$_{canopy}$	0.30	0.0040	16.7	1550_ske$_{canopy}$	0.14	0.0033	27.2
1550_max$_{canopy}$	0.30	0.0040	16.8	1550_range$_{canopy}$	0.13	0.0033	27.3
905_range$_{canopy}$	0.23	0.0042	17.5	NDI_entropy$_{canopy}$	0.13	0.0033	27.4

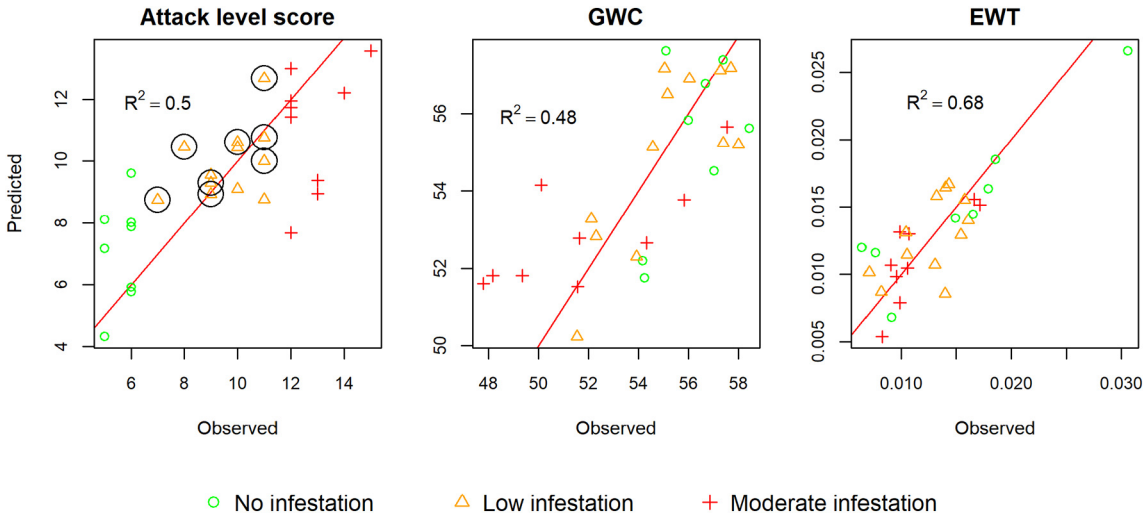

Fig. 7. Observed vs. predicted attack-level score, GWC, and EWT. The adjusted R^2 of the multiple-regression models is reported within the plots. Green attack trees (i.e., those with no visible discoloration) are circled in the attack-level score plot. (For interpretation of the references to color in this figure legend, the reader is referred to the web version of this article.)

TLS intensity in mapping EWT, as both are suitable for EWT estimation (Junttila et al., 2018; Zhu et al., 2017). This study's stepwise algorithm chose the following intensity features: 1550_kur$_{canopy}$, NDI_sd$_{canopy}$, and NDI_min$_{canopy}$. The selection of features based on the shape of the intensity-value distribution—rather than on statistics that depend on the scale of the value distribution (e.g., mean and percentiles)—is explained by the complications in the intensity calibration due to the varying effect that distance has on lidar intensity. The canopy-intensity metrics show only a weak relationship with GWC in this study.

LWC exhibits within-tree variation in this study; this is especially high for EWT, which shows vertical variation; it may be that, for each tree in the GWC and EWT reference data, the sampling rate does not sufficiently describe the variation of LWC in mature trees, thus hindering the development of more accurate regression models. TLS measures the entirety of the tree canopy that is visible from the scanner's point of view, so local variations in LWC can significantly affect the development of tree-wise regression models. The point-cloud classification could also have affected the results because it is difficult to quantify the effect that the woody material under the needles has on the intensity response.

4.4. Lidar intensity in response to I. typographus infestation

Various infestation symptoms influence a variety of dual-wavelength TLS intensity metrics. The single-predictor, ordinal, logistic-regression models indicate that the range and the maximum lidar intensity increase for both the 905 and 1550 nm wavelengths when there is a large amount of resin on the tree stem, thus indicating that resin can cause a strong and distinguishable backscatter. This could be due to the smooth and glossy surface of the resin, which could create a strong, mirror-like reflection that can be detected in the intensity distributions. The strongest predictors of crown discoloration are in the distributions of NDI and the 1550 nm wavelength, which are both sensitive to LWC (Gaulton et al., 2013; Junttila et al., 2018; Zhu et al., 2015). This result is in line with the finding that, of all the infestation symptoms, discoloration has the strongest relationship with GWC. Defoliation most affects the skewness of both the 1550 and 905 nm wavelengths, in addition to the range and maximum values of the 1550 nm wavelength. The reduction that the edge effect has on lidar intensity (as discussed above), as well as the alterations in reflectance, can explain the effect that defoliation has on the intensity-distribution skewness. The reduction in LWC in the defoliated tree canopies can explain this influence on the range and maximum of the 1550 nm wavelength, as there is a significant correlation between defoliation and GWC. In addition, researchers have previously observed increases in the reflectance of the 905 nm wavelength during bark beetles' green attack; this could be due to changes in the needles' cell structures (Cheng et al., 2010).

The relationship between infestation severity and lidar intensity was analyzed using two response variables: infestation class and attack-level score. Both analyses indicate that the 905_ske$_{canopy}$ intensity metric has the most predictive power, with the 1550_ske$_{canopy}$ and 1550_max$_{canopy}$ metrics in the following positions. Based on these analyses, the 905 nm wavelength seems to be more sensitive to bark-beetle infestation than the 1550 nm wavelength. This could be due to generally stronger reflectivity of Norway spruce needles in the 905 nm band, thus enabling observations in that band to detect more subtle changes than can be found in the 1550 nm band (Rautiainen et al., 2018).

4.5. The early detection of I. typographus infestations using lidar intensity

Dual-wavelength TLS were shown to detect *I. typographus* infestations even in the green-attack stage. This early detection was enabled by the application of intensity metrics from both the stem and the canopy as part of a LDA model. The separation of the *low* and *moderate*

Table 8
Summary of the regression analysis for the estimation of attack-level score, GWC, and EWT at tree level, with the p for each of the selected variables ($^{*}p < 0.001$; $^{**}p < 0.01$).

Independent variable	Explanatory variables	Models	Adjusted R^2	Predicted R^2	*RMSE*	*RMSE*%
Attack-level score	Canopy, stem	1550_ range$_{canopy}^{*}$, 905_range$_{stem}^{*}$, 1550_D75$_{canopy}^{**}$	0.50	0.44	1.95	19.5
GWC	Canopy, stem	NDI_kur$_{stem}^{*}$, 1550_D75$_{stem}^{**}$, 1550_p40$_{stem}^{**}$	0.48	0.36	2.03	19.1
GWC	Canopy	905_p80$_{canopy}^{**}$, 1550_D75$_{canopy}^{**}$	0.19	0.11	2.58	24.2
EWT	Canopy	1550_kur$_{canopy}^{*}$, NDI_sd$_{canopy}^{*}$, NDI_min$_{canopy}^{*}$	0.68	0.50	0.0026	10.7
EWT (without outliers)	Canopy	NDI_mean$_{canopy}^{*}$. NDI_min$_{canopy}^{*}$	0.39	0.35	0.0027	22.0

Table 9
Leave-one-out cross-validation results of the LDA classification for the three-class and two-class schemes (n = 29).

Three-class scheme					
Explanatory variables: NDI_kur_{canopy}, 905_range_{stem}, 905_ske_{canopy}					
	Classification				
	No infestation	Low infestation	Moderate infestation	Total	Producer accuracy (%)
Field control					
No infestation	6	2	0	8	75
Low infestation	1	8	3	12	67
Moderate infestation	1	3	5	9	56
Total	8	13	8	29	
User accuracy (%)	75	62	63		Overall accuracy: 66%

Two-class scheme				
Explanatory variables: 905_ske_{canopy}, 905_range_{stem}, 905_ske_{stem}				
	Classification			
	Not infested	Infested	Total	Producer accuracy (%)
Field control				
Not infested	6	2	8	75
Infested	1	20	21	95
Total	7	22	29	
User accuracy (%)	86	91		Overall accuracy: 90%

infestation classes was only moderately successful, with an overall classification accuracy of 66%. The two-class classification scheme (*not infested* and *infested*) showed an overall classification accuracy of 90%. However, it should be noted that the balance of trees within each class was unequal, which increased the measured overall classification accuracy. The producer's accuracy for the *not infested* class was 75% for both classification schemes. These results are encouraging, but more research is required to further evaluate the accuracy of this method because the sample size was small and because there was no separate test data set to provide an independent assessment of the classification accuracy. A large data set with hundreds or thousands of trees would enable the employment of machine-learning techniques that could assist in harnessing the full potential of the high-resolution multispectral TLS data for the reflectance and structural variables.

The multiple-regression model shows fair agreement between the attack-level score and the lidar intensity metrics (R^2 = 0.50, *RMSE* = 1.95), further indicating the potential of using lidar intensity in assessments of infestation severity; the data was characterized only by *low* and *moderate* damage, however. The variables for the stepwise algorithm differed slightly from the selected LDA variables due to the former's different data-fitting approach (multiple regression), but the selected variables did include the 905_range_{stem} feature, which shows predictive power for detecting resin flows. All the developed multiple-regression models employ more metrics that describe the shape of the value distribution (in terms of kurtosis, skewness, and density) than actual values (e.g., means or percentiles). This is an interesting result because it indicates that absolute radiometric calibration between data sets may not be necessary for the detection of bark-beetle infestations;

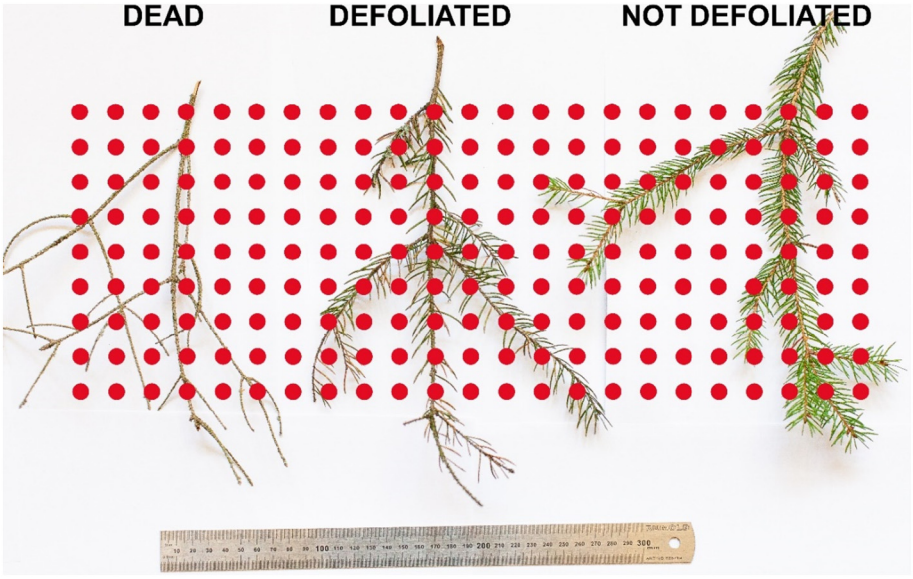

Fig. 8. Illustration of dead, defoliated, and undefoliated branches with laser-beam diameters (to scale) for a distance of 20 m using the 905 nm wavelength.

this would simplify the preprocessing requirements.

TLS and other terrestrial lidar techniques (e.g., mobile lidar systems) are also increasingly common in operational forest inventories in both the public and private sectors, largely due to their ability to describe forest structures accurately (Liang et al., 2018). In the future, lidar sensors will likely be integrated into harvesters, thus assisting drivers in the selection and partitioning of trees and enabling the collection of vast amounts of data on the remaining trees (Liang et al., 2014). As lidar sensors develop, their prices will drop, and their sizes will decrease, allowing for an increasing in multispectral applications and enabling simultaneous measurements of trees' vigor and structure (Eitel et al., 2016). The collection of such data could aid in the large-area mapping of forest health by providing ground-truth data for use in training models based on, for instance, satellite imagery. As an example, Sentinel-2 images have shown potential for the early detection of *I. typographus* when the infected area is large, but such models still require ground-reference data for calibration and validation (Abdullah et al., 2019). Based on the results of this study, TLS intensity has potential for the objective assessment of trees' condition and health, despite the relatively small sample size of this study. This method should thus be further investigated. The method could be improved by, for instance, combining intensity metrics with structural metrics that better assess defoliation levels and that thus better distinguish the severity of a tree's decline. The lidar-intensity calibration for coniferous trees also requires further research so as to eliminate some of the random variation and improve the usability of the data. In addition, the stability of the various intensity metrics across multiple data-acquisition scenarios—in which scanning angles can vary and cause changes in viewing positions—should be investigated.

This is the first step toward the development of a single-sensor solution for simultaneously measuring trees' structure and vigor. TLS shows the ability to detect early bark-beetle colonization, which could enable forest managers to predict bark-beetle infestations at higher accuracy so that they can take preemptive measures to prevent further forest damage and to mitigate the existing damage, such as by conducting salvage cuttings to remove infested trees. Up-to-date information on tree vigor could also help identify which trees are most vulnerable to bark-beetle attacks; such trees could then be removed when the risk of a bark-beetle outbreak is high. In future studies, researchers should focus on improving the distance calibration of TLS intensity for targets that cause multiple scattering, such as coniferous species, as well as on comparing multispectral TLS to other lidar-sensor platforms across a variety of tree species, symptoms, and causes of tree decline or damage.

Acknowledgments

Funding

This work was supported by the Academy of Finland project Centre of Excellence in Laser Scanning Research (CoE-LaSR) under [grant number 307362], the Finnish Cultural Foundation and the Niemi Foundation. Stora Enso Ltd. and Tornator Ltd., particularly Jarmo Hakalisto and Maarit Sallinen are thanked for enabling our study in Viitalampi.

Appendix A. Supplementary data

Supplementary data associated with this article can be found in the online version, at doi:https://doi.org/10.1016/j.rse.2019.111264. These data include the Google map of the most important areas described in this article.

References

Abdullah, H., Darvishzadeh, R., Skidmore, A.K., Groen, T.A., Heurich, M., 2018. European spruce bark beetle (Ips typographus, L.) green attack affects foliar reflectance and biochemical properties. Int. J. Appl. Earth Obs. Geoinf. 64, 199–209.

Abdullah, H., Skidmore, A.K., Darvishzadeh, R., Heurich, M., 2019. Sentinel-2 accurately maps green-attack stage of European spruce bark beetle (Ips typographus, L.) compared with Landsat-8. Remote Sens. Ecol. Conserv. 5 (1), 87–106.

Agresti, A., 2002. Categorical Data Analysis. John Wiley & Sons. Inc., Publication.

Agresti, A., Tarantola, C., 2018. Simple ways to interpret effects in modeling ordinal categorical data. Statistica Neerlandica 72, 210–223.

Allen, C.D., Macalady, A.K., Chenchouni, H., Bachelet, D., McDowell, N., Vennetier, M., Kitzberger, T., Rigling, A., Breshears, D.D., Hogg, E., 2010. A global overview of drought and heat-induced tree mortality reveals emerging climate change risks for forests. For. Ecol. Manag. 259, 660–684.

Allen, C.D., Breshears, D.D., McDowell, N.G., 2015. On underestimation of global vulnerability to tree mortality and forest die-off from hotter drought in the Anthropocene. Ecosphere 6, 1–55.

Austin, P.C., Steyerberg, E.W., 2015. The number of subjects per variable required in linear regression analyses. J. Clin. Epidemiol. 68, 627–636.

Balduzzi, M.A., Van der Zande, D., Stuckens, J., Verstraeten, W.W., Coppin, P., 2011. The properties of terrestrial laser system intensity for measuring leaf geometries: a case study with conference pear trees (Pyrus Communis). Sensors 11, 1657–1681.

Blomqvist, M., Kosunen, M., Starr, M., Kantola, T., Holopainen, M., Lyytikäinen-Saarenmaa, P., 2018. Modelling the predisposition of Norway spruce to Ips typographus L. infestation by means of environmental factors in southern Finland. Eur. J. For. Res. 1–17.

Brodu, N., Lague, D., 2012. 3D terrestrial lidar data classification of complex natural scenes using a multi-scale dimensionality criterion: applications in geomorphology. ISPRS J. Photogramm. Remote Sens. 68, 121–134.

Carnicer, J., Coll, M., Ninyerola, M., Pons, X., Sanchez, G., Penuelas, J., 2011. Widespread crown condition decline, food web disruption, and amplified tree mortality with increased climate change-type drought. Proc. Natl. Acad. Sci. 108, 1474–1478.

Ceccato, P., Flasse, S., Tarantola, S., Jacquemoud, S., Grégoire, J.-M., 2001. Detecting vegetation leaf water content using reflectance in the optical domain. Remote Sens. Environ. 77, 22–33.

Cheng, T., Rivard, B., Sánchez-Azofeifa, G., Feng, J., Calvo-Polanco, M., 2010. Continuous wavelet analysis for the detection of green attack damage due to mountain pine beetle infestation. Remote Sens. Environ. 114, 899–910.

Coulson, R.N., Amman, G.D., Dahlsten, D.L., DeMars Jr., C., Stephen, F., 1985. Forest-Bark Beetle Interactions: Bark Beetle Population Dynamics. Integrated Pest Management in Pine-Bark Beetle Ecosystems. John Wiley & Sons, New York, pp. 61–80.

Danson, F., Steven, M., Malthus, T., Clark, J., 1992. High-spectral resolution data for determining leaf water content. Int. J. Remote Sens. 13, 461–470.

Datt, B., 1999. Remote sensing of water content in Eucalyptus leaves. Aust. J. Bot. 47, 909–923.

Davies, O.L., 1947. Statistical Methods in Research and Production. Statistical Methods in Research and Production.

Douglas, E.S., Strahler, A., Martel, J., Cook, T., Mendillo, C., Marshall, R., Chakrabarti, S., Schaaf, C., Woodcock, C., Li, Z., 2012. DWEL: a dual-wavelength echidna lidar for ground-based forest scanning. In: IEEE International Geoscience and Remote Sensing Symposium (IGARSS), pp. 4998–5001.

Eitel, J.U., Vierling, L.A., Long, D.S., 2010. Simultaneous measurements of plant structure and chlorophyll content in broadleaf saplings with a terrestrial laser scanner. Remote Sens. Environ. 114, 2229–2237.

Eitel, J.U., Vierling, L.A., Long, D.S., Hunt, E.R., 2011. Early season remote sensing of wheat nitrogen status using a green scanning laser. Agric. For. Meteorol. 151, 1338–1345.

Eitel, J.U., Magney, T.S., Vierling, L.A., Brown, T.T., Huggins, D.R., 2014. LiDAR based biomass and crop nitrogen estimates for rapid, non-destructive assessment of wheat nitrogen status. Field Crop Res. 159, 21–32.

Eitel, J.U., Höfle, B., Vierling, L.A., Abellán, A., Asner, G.P., Deems, J.S., Glennie, C.L., Joerg, P.C., LeWinter, A.L., Magney, T.S., 2016. Beyond 3-D: the new spectrum of lidar applications for earth and ecological sciences. Remote Sens. Environ. 186, 372–392.

Elsherif, A., Gaulton, R., Mills, J., 2018. Estimation of vegetation water content at leaf and canopy level using dual-wavelength commercial terrestrial laser scanners. Interface Ffocus. 8, 20170041.

Eriksson, M., Neuvonen, S., Roininen, H., 2007. Retention of wind-felled trees and the risk of consequential tree mortality by the European spruce bark beetle Ips typographus in Finland. Scand. J. For. Res. 22, 516–523.

Errington, A.F., Daku, B.L., 2017. Temperature compensation for radiometric correction of terrestrial LiDAR intensity data. Remote Sens. 9, 356.

Faccoli, M., 2009. Effect of weather on Ips typographus (Coleoptera Curculionidae) phenology, voltinism, and associated spruce mortality in the southeastern Alps. Environ. Entomol. 38, 307–316.

Fassnacht, F.E., Latifi, H., Ghosh, A., Joshi, P.K., Koch, B., 2014. Assessing the potential of hyperspectral imagery to map bark beetle-induced tree mortality. Remote Sens. Environ. 140, 533–548.

Gardiner, B., Blennow, K., Carnus, J.-M., Fleischer, P., Ingemarson, F., Landmann, G., Lindner, M., Marzano, M., Nicoll, B., Orazio, C., 2010. Destructive Storms in European Forests: Past and Forthcoming Impacts. European Forest Institute, Joensuu, Finland.

Gaulton, R., Danson, F., Ramirez, F., Gunawan, O., 2013. The potential of dual-wavelength laser scanning for estimating vegetation moisture content. Remote Sens. Environ. 132, 32–39.

Girardeau-Montaut, D., 2011. Cloudcompare-Open Source Project. OpenSource Project.

Gregow, H., Laaksonen, A., Alper, M., 2017. Increasing large scale windstorm damage in

Western, Central and Northern European forests, 1951–2010. Sci. Rep. 7, 46397.
Hakala, T., Suomalainen, J., Kaasalainen, S., Chen, Y., 2012. Full waveform hyperspectral LiDAR for terrestrial laser scanning. Opt. Express 20, 7119–7127.
Hoque, E., Hutzler, P., Hiendl, H., 1990. Studies on reflective features of Norway spruce and their possible applications in remote sensing of forest damage. Toxicol. Environ. Chem. 27, 209–215.
Hunt Jr., E.R., Rock, B.N., 1989. Detection of changes in leaf water content using near- and middle-infrared reflectances. Remote Sens. Environ. 30, 43–54.
Immitzer, M., Atzberger, C., 2014. Early detection of bark beetle infestation in Norway spruce (Picea abies, L.) using worldView-2 data frühzeitige erkennung von borkenkä ferbefall an fichten mittels worldView-2 satellitendaten. Photogrammetrie-Fernerkundung-Geoinformation 2014, 351–367.
Junttila, S., Vastaranta, M., Liang, X., Kaartinen, H., Kukko, A., Kaasalainen, S., Holopainen, M., Hyyppä, H., Hyyppä, J., 2016. Measuring leaf water content with dual-wavelength intensity data from terrestrial laser scanners. Remote Sens. 9.
Junttila, S., Sugano, J., Vastaranta, M., Linnakoski, R., Kaartinen, H., Kukko, A., Holopainen, M., Hyyppä, H., Hyyppä, J., 2018. Can leaf water content be estimated using multispectral terrestrial laser scanning? A case study with Norway spruce seedlings. Front. Plant Sci. 9, 299.
Kaasalainen, S., Hyyppä, H., Kukko, A., Litkey, P., Ahokas, E., Hyyppä, J., Lehner, H., Jaakkola, A., Suomalainen, J., Akujärvi, A., 2009. Radiometric calibration of LIDAR intensity with commercially available reference targets. IEEE Trans. Geosci. Remote Sens. 47, 588–598.
Kaasalainen, S., Hyyppä, J., Karjalainen, M., Krooks, A., Lyytikäinen-Saarenmaa, P., Holopainen, M., Jaakkola, A., 2010. Comparison of terrestrial laser scanner and synthetic aperture radar data in the study of forest defoliation. In: ISPRS TC VII Symposium – 100 Years ISPRS, Vienna, Austria, July 5–7, 2010, IAPRS, Vol. XXXVIII, Part 7A, pp. 82–87.
Kaasalainen, S., Jaakkola, A., Kaasalainen, M., Krooks, A., Kukko, A., 2011. Analysis of incidence angle and distance effects on terrestrial laser scanner intensity: search for correction methods. Remote Sens. 3, 2207–2221.
Kaasalainen, S., Nevalainen, O., Hakala, T., Anttila, K., 2016. Incidence angle dependency of leaf vegetation indices from hyperspectral lidar measurements. Photogrammetrie-Fernerkundung-Geoinformation 2016, 75–84.
Kaasalainen, S., Åkerblom, M., Nevalainen, O., Hakala, T., Kaasalainen, M., 2018. Uncertainty in multispectral lidar signals caused by incidence angle effects. Interface Ffocus. 8, 20170033.
Kärvemo, S., Johansson, V., Schroeder, M., Ranius, T., 2016. Local colonization-extinction dynamics of a tree-killing bark beetle during a large-scale outbreak. Ecosphere 7, e01257.
Korpela, I., 2017. Acquisition and evaluation of radiometrically comparable multi-footprint airborne LiDAR data for forest remote sensing. Remote Sens. Environ. 194, 414–423.
Lange, H., Økland, B., Krokene, P., 2006. Thresholds in the life cycle of the spruce bark beetle under climate change. Interj. Complex Syst. 1648.
Långström, B., Lindelöw, Å., Schroeder, M., Björklund, N., Öhrn, P., 2009. The Spruce Bark Beetle Outbreak in Sweden Following the January-Storms in 2005 and 2007.
Lausch, A., Heurich, M., Gordalla, D., Dobner, H.-J., Gwillym-Margianto, S., Salbach, C., 2013. Forecasting potential bark beetle outbreaks based on spruce forest vitality using hyperspectral remote-sensing techniques at different scales. For. Ecol. Manag. 308, 76–89.
Leys, C., Ley, C., Klein, O., Bernard, P., Licata, L., 2013. Detecting outliers: do not use standard deviation around the mean, use absolute deviation around the median. J. Exp. Soc. Psychol. 49, 764–766.
Liang, X., Kankare, V., Yu, X., Hyyppa, J., Holopainen, M., 2014. Automated stem curve measurement using terrestrial laser scanning. IEEE Trans. Geosci. Remote Sens. 52, 1739–1748.
Liang, X., Kankare, V., Hyyppä, J., Wang, Y., Kukko, A., Haggrén, H., Yu, X., Kaartinen, H., Jaakkola, A., Guan, F., 2016. Terrestrial laser scanning in forest inventories. ISPRS J. Photogramm. Remote Sens. 115, 63–77.
Liang, X., Hyyppä, J., Kaartinen, H., Lehtomäki, M., Pyörälä, J., Pfeifer, N., Holopainen, M., Brolly, G., Francesco, P., Hackenberg, J., 2018. International benchmarking of terrestrial laser scanning approaches for forest inventories. ISPRS J. Photogramm. Remote Sens. 144, 137–179.
Linnakoski, R., Sugano, J., Junttila, S., Pulkkinen, P., Asiegbu, F.O., Forbes, K.M., 2017. Effects of water availability on a forestry pathosystem: fungal strain-specific variation in disease severity. Sci. Rep. 7, 13501.
Lorio Jr., P.L., Hodges, J.D., 1968. Oleoresin exudation pressure and relative water content of inner bark as indicators of moisture stress in loblolly pines. For. Sci. 14, 392–398.
Marini, L., Økland, B., Jönsson, A.M., Bentz, B., Carroll, A., Forster, B., Grégoire, J.c., Hurling, R., Nageleisen, L.M., Netherer, S., 2017. Climate drivers of bark beetle outbreak dynamics in Norway spruce forests. Ecography 40, 1426–1435.
McFadden, D., 1973. Conditional Logit Analysis of Qualitative Choice Behavior.
Näsi, R., Honkavaara, E., Lyytikäinen-Saarenmaa, P., Blomqvist, M., Litkey, P., Hakala, T., Viljanen, N., Kantola, T., Tanhuanpää, T., Holopainen, M., 2015. Using UAV-based photogrammetry and hyperspectral imaging for mapping bark beetle damage at tree-level. Remote Sens. 7, 15467–15493.
Niemann, K.O., Quinn, G., Stephen, R., Visintini, F., Parton, D., 2015. Hyperspectral remote sensing of mountain pine beetle with an emphasis on previsual assessment. Can. J. Remote. Sens. 41, 191–202.
Niu, Z., Xu, Z., Sun, G., Huang, W., Wang, L., Feng, M., Li, W., He, W., Gao, S., 2015. Design of a new multispectral waveform lidar instrument to monitor vegetation. IEEE Geosci. Remote Sens. Lett. 12, 1506–1510.
Økland, B., Berryman, A., 2004. Resource dynamic plays a key role in regional fluctuations of the spruce bark beetles Ips typographus. Agric. For. Entomol. 6, 141–146.
Peñuelas, J., Pinol, J., Ogaya, R., Filella, I., 1997. Estimation of plant water concentration by the reflectance water index WI (R900/R970). Int. J. Remote Sens. 18, 2869–2875.
Poorter, H., Niinemets, Ü., Poorter, L., Wright, I.J., Villar, R., 2009. Causes and consequences of variation in leaf mass per area (LMA): a meta-analysis. New Phytol. 182, 565–588.
R Core Team, 2013. A Language and Environment for Statistical Computing. R Foundation for Statistical Computing, Vienna, Austria.
Rautiainen, M., Lukeš, P., Homolová, L., Hovi, A., Pisek, J., Mottus, M., 2018. Spectral properties of coniferous forests: a review of in situ and laboratory measurements. Remote Sens. 10, 207.
Ripley, B., Venables, B., Bates, D.M., Hornik, K., Gebhardt, A., Firth, D., Ripley, M.B., 2013. Package 'Mass'. Cran R.
Royston, J.P., 1982. An extension of Shapiro and Wilk's W test for normality to large samples. J. R. Stat. Soc.: Ser. C: Appl. Stat. 31, 115–124.
Schwarz, G., 1978. Estimating the dimension of a model. Ann. Stat. 6, 461–464.
Seidl, R., Rammer, W., 2017. Climate change amplifies the interactions between wind and bark beetle disturbances in forest landscapes. Landsc. Ecol. 32, 1485–1498.
Shannon, C.E., 2001. A mathematical theory of communication. ACM SIGMOBILE Mob. Comput. Commun. Rev. 5, 3–55.
Silverman, B.W., 2018. Density Estimation for Statistics and Data Analysis. Routledge.
Sturrock, R., Frankel, S., Brown, A., Hennon, P., Kliejunas, J., Lewis, K., Worrall, J., Woods, A., 2011. Climate change and forest diseases. Plant Pathol. 60, 133–149.
Tan, K., Cheng, X., Ding, X., Zhang, Q., 2016. Intensity data correction for the distance effect in terrestrial laser scanners. IEEE J. Sel. Top. Appli. Earth Obs. Remote Sens. 9, 304–312.
Trumbore, S., Brando, P., Hartmann, H., 2015. Forest health and global change. Science 349, 814–818.
Wagner, W., Ullrich, A., Ducic, V., Melzer, T., Studnicka, N., 2006. Gaussian decomposition and calibration of a novel small-footprint full-waveform digitising airborne laser scanner. ISPRS J. Photogramm. Remote Sens. 60, 100–112.
Waring, R.H., 1983. Estimating forest growth and efficiency in relation to canopy leaf area. Adv. Ecol. Res. 327–354 (Elsevier).
Watson, G., 2006. Computing Helmert transformations. J. Comput. Appl. Math. 197, 387–394.
Wermelinger, B., 2004. Ecology and management of the spruce bark beetle *Ips typographus* — a review of recent research. For. Ecol. Manag. 202, 67–82.
Wong, C.M., Daniels, L.D., 2017. Novel forest decline triggered by multiple interactions among climate, an introduced pathogen and bark beetles. Glob. Chang. Biol. 23, 1926–1941.
Zhu, X., Wang, T., Darvishzadeh, R., Skidmore, A.K., Niemann, K.O., 2015. 3D leaf water content mapping using terrestrial laser scanner backscatter intensity with radiometric correction. ISPRS J. Photogramm. Remote Sens. 110, 14–23.
Zhu, X., Wang, T., Skidmore, A.K., Darvishzadeh, R., Niemann, K.O., Liu, J., 2017. Canopy leaf water content estimated using terrestrial LiDAR. Agric. For. Meteorol. 232, 152–162.
Zhu, X., Skidmore, A.K., Wang, T., Liu, J., Darvishzadeh, R., Shi, Y., Premier, J., Heurich, M., 2018. Improving leaf area index (LAI) estimation by correcting for clumping and woody effects using terrestrial laser scanning. Agric. For. Meteorol. 263, 276–286.
Zuur, A.F., Ieno, E.N., Elphick, C.S., 2010. A protocol for data exploration to avoid common statistical problems. Methods Ecol. Evol. 1, 3–14.